Chinese Chemical Letters 34 (2023) 107510

Contents lists available at ScienceDirect

Chinese Chemical Letters

journal homepage: www.elsevier.com/locate/cclet

A colorimetric assay for cholesterol based on the encapsulation of multienzyme in leaf-shape crossed ZIF-L

Jiaqi He[a], Tingling Zhuo[a], Yintong Teng[b], Guoqin Chen[a,*], Peng Zhao[c,e,*], Caiwen Ou[b,d,e,*]

[a] Department of Cardiology, Guangzhou Panyu Central Hospital, Guangzhou University of Chinese Medicine, Guangzhou 510006, China
[b] Department of Cardiology and Laboratory of Heart Center, Zhujiang Hospital, Southern Medical University, Guangzhou 510280, China
[c] NMPA Key Laboratory for Research and Evaluation of Drug Metabolism, Guangdong Provincial Key Laboratory of New Drug Screening, School of Pharmaceutical Sciences, Southern Medical University, Guangzhou 510515, China
[d] Affiliated Dongguan Hospital, Southern Medical University, Dongguan 523059, China
[e] Guangdong Provincial Key Laboratory of Shock and Microcirculation, Southern Medical University, Guangzhou 510515, China

ARTICLE INFO

Article history:
Received 13 January 2022
Revised 2 May 2022
Accepted 10 May 2022
Available online 14 May 2022

Keywords:
Cholesterol
Zeolitic imidazolate framework-L
Artificial enzyme
Colorimetric
Point-of-care testing

ABSTRACT

The serum cholesterol level is an important indicator of healthy and there is a great necessity for frequent cholesterol monitoring to some cardiovascular-related diseases, which puts forward higher requirements for point-of-care testing (POCT) of cholesterol. In this work, a cascade catalytic system of cholesterol is developed by encapsulation of cholesterol oxidase (ChOx) and PdCuAu nanoparticles into zeolitic imidazolate framework-L (ChOx/PCA@ZIF-L). Results indicate that ZIF-L carrier can significantly increase the catalytic activity of single or multiple enzymes, due to its high loading capacity and efficient molecular transport. Under the optimal conditions, the absorbance of reaction system performs linear relationships with the concentration of cholesterol in two intervals from 0.0005 mmol/L to 1.0000 mmol/L, with a limit of detection of 0.2176 μmol/L. The proposed colorimetric strategy based on ChOx/PCA@ZIF-L performs a good agreement with the results provided by chemiluminescence method for the serum cholesterol detection. Interestingly, a simple paper-based sensing system is constructed through a pre-reaction-transfer operation, which gets rid of the complex pre-processing requirements of traditional operations on filter paper. The presented strategy allows for the sensitive, convenient, costless assay of serum cholesterol, and paves a new way to design the POCT device for daily monitoring of healthy.

Cholesterol, a derivative of cyclopentane polyhydrophenanthrene, serves as a precursor for the synthesis of many important substances in living organisms such as bile acids, hormones, and vitamin D [1]. In addition, cholesterol also participates in the formation of cell membranes and maintenance of normal physiological functions of cell membranes [2]. The appropriate level of total cholesterol in the serum of healthy adults should be less than 5.2 mmol/L. Yet with the change in people's dietary habits and lifestyles, the incidence of dyslipidemia has increased significantly [3]. Researchers found that hypercholesteremia had been repositioned globally, shifting from high-income countries such as north America to east and southeast Asia [4]. Among them, the overall prevalence of dyslipidemia in Chinese adults is as high as 40.40%, which is a significant increase from 2002 [5]. Plenty of researches show that excessive serum cholesterol levels are closely related to the occurrence of arteriosclerosis, cerebral thrombosis, and coronary heart disease [6]. According to statistics, every 1% reduction of cholesterol content in serum reduces the risk of heart disease by 2% [7].

At present, many analytical technologies have been developed to detect cholesterol, the common ones are liquid chromatography-mass spectrometry (LC-MS) [8], electrochemical methods [9,10], fluorescence spectrometry [11,12], colorimetry [13–15], *etc*. Compared with other methods, colorimetry is a convenient and economical detection method, which can get rid of the need of professional instruments, and is suitable for on-site diagnosis. The colorimetric detection of cholesterol is mainly based on the cascaded enzyme-catalyzed reactions, in which the produced H_2O_2 oxidizes the colorless 3,3′,5,5′-tetramethylbenzidine (TMB) into blue oxTMB [16]. In order to realize the efficient cascaded reactions, the immobilization of the enzymes is one of the most attractive strategies as their improved operation stability, easier reactor operation, and being recycled to reduce the production cost [17].

* Corresponding authors.
E-mail addresses: chenguoqin1@163.com (G. Chen), smuzp@smu.edu.cn (P. Zhao), oucaiwen@smu.edu.cn (C. Ou).

https://doi.org/10.1016/j.cclet.2022.05.024
1001-8417/

Multiple carriers were developed for the enzyme immobilization such as chitosan [18], halloysite [19], silica [20], carbon nanotubes [21], and porous materials [22–24]. Metal-organic frameworks (MOFs) are a new type of porous materials with metal-containing nodes and organic ligands linked through coordination bonds [25]. Because of their high surface area and tunable pore size, MOFs have served as potent supporting matrices for enzyme immobilization in biosensing, diagnosis, treatment of diseases, *etc*. [26–28]. In the design of MOFs-based enzyme catalytic systems, the pore size of MOFs is a key factor affecting the catalytic activity of an enzyme [29]. Among the different MOFs, the two-dimensional (2D) zeolitic imidazolate framework-L (ZIF-L) exhibits a leaf-like morphology and large pore cavities between its unique 2D layered structures [30,31]. Cui *et al*. reported the synthesis of catalase@ZIF with cruciate flower-like morphology under high concentration Zn^{2+} and 2-methylimidazole [32]. Benefiting from its large mesopore size and high protein loading capacity, the catalytic activity of flower-like catalase@ZIF exhibited 400% higher than that of conventional rhombic dodecahedral morphology. Liu *et al*. had constructed separated organelles of the cell mimics by separately encapsulating glucose oxidase (GOx) and peroxidase from horseradish (HRP) in ZIF-L nanoparticles [33]. Various cellular mimicking events including metabolism, communication, and programmed degradation were successfully realized, resulting from the efficient molecular transport properties of ZIF-L. Therefore, the ZIF-L is suitable for enzyme immobilization to determine cholesterol, however, the effect of ZIF-L on cholesterol cascade catalysis has never been reported.

In recent years, portable test devices for serum cholesterol are in great necessity as daily monitoring of cholesterol and become increasingly important, the development of point-of-care testing (POCT) is in full swing [34,35]. Among the various supporting materials for POCT of cholesterol, the paper-based devices are the most affordable, which are especially for applications in resource-limited areas when combined with using a smartphone as a detector [36]. Nanoscale artificial enzymes have attracted extensive attention from scholars attributed to their advantages of simple preparation, low cost, and high stability [37–39]. Pd element contained nanoparticles with unique electronic properties and high catalytic activity have been considered as promising peroxidase (POD)-like nano-enzyme in biosensors fabrication [40,41]. Thus, the introduction of artificial enzymes in the cascade catalytic reaction on POCT devices of cholesterol may ensure the detection stability and ease the preparation processes.

Herein, we presented the co-precipitation approach to immobilize ChOx and PdCuAu alloy nanoparticles in leaf-liked ZIF-L (ChOx/PCA@ZIF-L). The cholesterol was oxidized by oxygen in the presence of ChOx to produce cholest-4-en-3-one and H_2O_2. Then, PdCuAu alloy nanoparticles with POD-like activity catalyzed the oxidation of peroxidase substrate TMB by H_2O_2 to produce a blue color product (Scheme 1). It was found that the cascade catalytic efficiency could be improved by ZIF-L compared with conventional ZIF-8 and free enzymes. Under the optimal conditions, the ChOx/PCA@ZIF-L was available for the sensitive and specific detection of cholesterol in buffer and serum of patients with dyslipidemia. Furthermore, when combined with the paper sensing system, the POC detection of serum cholesterol is presented to serve as an efficient and rapid approach for the diagnosis of hypercholesterolemia.

In order to construct the cascade catalytic nanocomposite, the PdCuAu nanoparticles were firstly obtained through hydrothermal reduction reaction containing three metal ions and ascorbic acid. Then, the ChOx/PCA@ZIF-L was synthesized by the co-precipitation with the high concentrations of Zn^{2+} and 2-methylimidazole. While self-assembled to form the carrier, the two were directly sealed to ZIF-L. The morphology of the synthesized nanocomposites was analyzed using SEM and TEM. The TEM results showed that the obtained PdCuAu nanoparticles (Fig. S1 in Supporting information) were spherical and uniform (average diameter: 10 nm). However, due to the small diameter of the nanoparticles, the specific surface area and surface energy increase, will increase the probability of agglomeration [42]. It could be seen that the bare PdCuAu NPs were aggregate. As shown in Fig. 1A, the prepared ZIF-L was sheet-like and crossed with a length of 2.8 μm, a center width of 1.0 μm, and a thickness of 50 nm. Fig. 1B showed the TEM image of ChOx/PCA@ZIF-L. It could be observed that the high density of small particles on the ZIF-L by local magnification. In addition, the ChOx/PCA@ZIF-L composite presented the same leaf-like crystal morphology as pure ZIF-L, which suggested that the presence of PdCuAu nanoparticles and ChOx neither inhibited the crystallization of ZIF-L, nor affected the crystal shape of ZIF-L. Furthermore, the SEM images of ZIF-L and ChOx/PCA@ZIF-L were exhibited in Figs. 1C and D, which were in line with the TEM characterization.

Next, the phase composition and crystal structure of the composites were characterized by XRD with a scanning angle of 10°∼50° and a scanning speed of 2°/min. The main diffraction peaks of ZIF-L (Fig. 2A) were observed at 2θ values of 10.98°, 12.7°, 15.12°, 18.0° and 28.98°, which correspond to the (020), (220), (400), (004), and (800) planes, respectively. The XRD pattern of ZIF-L matched well with this of simulated ZIF-L (CCDC database identifier: IWOZOL), indicating that ZIF-L was successfully synthesized. It is noted that the diffractions of PdCuAu nanoparticles can not be detected in the XRD pattern of PCA@ZIF-L and ChOx/PCA@ZIF-L, this is due to their ultrasmall size and high dispersion in the ZIF-L [43,44]. Furthermore, the XRD pattern of ChOx/PCA@ZIF-L composites resembled that of pure ZIF-L, revealing that there was no significant difference with regard to the crystal structure and crystallinity following ChOx immobilization.

The functional groups of ZIF-L, PCA@ZIF-L, and ChOx/PCA@ZIF-L were analyzed by FT-IR in Fig. 2B. The bands at 3133 cm^{-1}, 2972 cm^{-1}, and 2927 cm^{-1} were attributed to the C-H stretch on the imidazole. The characteristic peaks at 1565 cm^{-1} and around 1050 cm^{-1} were ascribed to the C=N double bond, bending vibration of C-H on the imidazole, respectively [45]. The absorption peak at 754 cm^{-1} was corresponded to the coordination between the ZIF skeleton and imidazole N atoms forming the Zn-N bond [46]. Additionally, the peak at 840 cm^{-1} is due to the presence of Zn-O. The peak at 1658 cm^{-1} was mainly from C=O stretching mode, indicating the presence of proteins in the composites [47]. Comparing three spectra, the all bands appeared at the same position, which indicated the existence of the same chemical bonding on them.

The composition and valence of elements in the ZIF-L and ChOx/PCA@ZIF-L were measured by XPS. As anticipated, the XPS wide-scan spectra (Fig. S2A in Supporting information) confirmed that ZIF-L contained four major elements, including C, O, N and Zn. Compared with ZIF-L, ChOx/PCA@ZIF-L had three more elements, Cu, Au, and Pd (Fig. S2B in Supporting information). The characteristic peaks of Cu and Pd were not obvious, which was mainly due to the low content of Cu and Pd. In a high-resolution scan, two characteristic peaks of Zn appeared at 1045.0 and 1021.9 eV (Fig. 2C), which were assigned to Zn $2p_{1/2}$ and $2p_{3/2}$, respectively. The high-resolution N 1s spectra (Fig. 2D) could be fitted to three different bands.

The N_2 sorption-desorption isotherms analysis (Fig. 2E) showed that the hysteresis loops were clearly observed at a lower relative pressure range ($P/P_0 > 0.2$), which indicated the presence of mesoporous structures of the ZIF-L and ChOx/PCA@ZIF-L composites. Pore diameter distribution was calculated using Barrett-Joyner-Halenda (BJH) models based on the adsorption isotherm. The inset in Fig. 2E showed that the pore size distribution of ZIF-L and ChOx/PCA@ZIF-L was centered at 11 nm. Compared to ZIF-

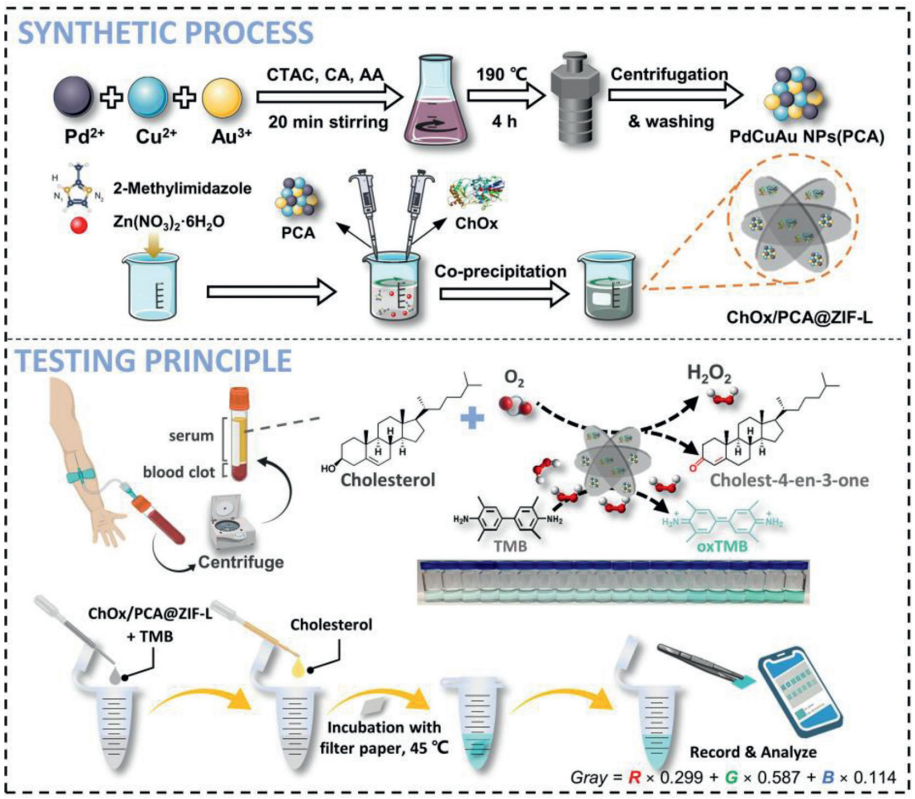

Scheme 1. Schematic diagrams of ChOx/PCA@ZIF-L synthesis, catalytic oxidation principle of cholesterol, and the cholesterol detection using ChOx/PCA@ZIF-L-based test paper.

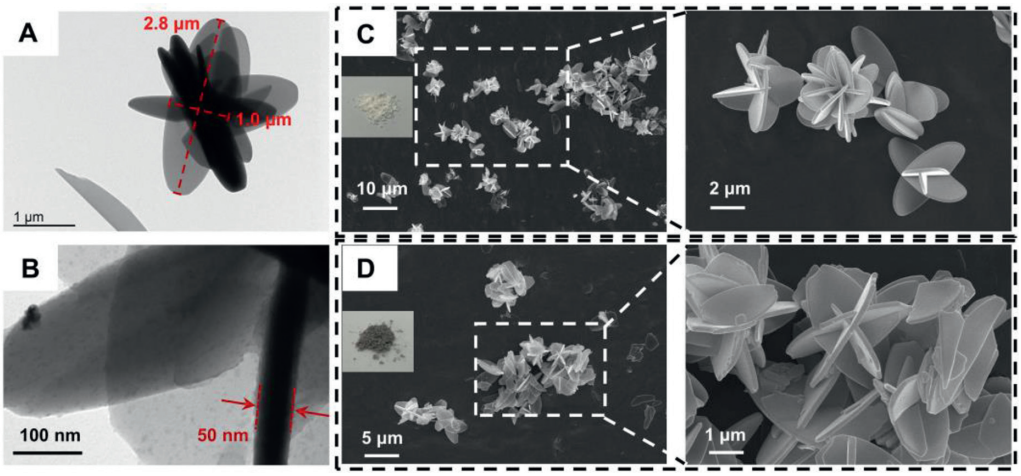

Fig. 1. TEM images of (A) ZIF-L and (B) ChOx/PCA@ZIF-L. SEM images of (C) ZIF-L and (D) ChOx/PCA@ZIF-L with partially enlarged results. Insets in (C) and (D) are the digital photos of ZIF-L and ChOx/PCA@ZIF-L powders, relatively.

8 (Fig. S3 in Supporting information), however, the surface area and pore volume of ZIF-L were lower. This is because ZIF-L has higher density (density of metal atoms per unit volume) than ZIF-8. Moreover, cavities in ZIF-L are much more flexible than the rhombic dodecahedral structure of ZIF-8, because they are located between the 2D layers that are weakly connected by the terminal methylimidazole-4 and "free" methylimidazole-5 [48]. Therefore, ZIF-L possesses superior adsorption selectivity and could enable an efficient molecular transportation and cascade catalytic reaction of cholesterol.

The POD-like property of PCA@ZIF-L was studied using the reaction of oxidizing the chromogenic substrate TMB. As illustrated in Fig. 2F, the colorless TMB solution rapidly changed into blue with the introduction of the PCA@ZIF-L composites and H_2O_2 (Fig. 2F inset) because of the produced hydroxyl radicals, where a characteristic absorbance at 652 nm appeared, like that of horseradish peroxidase (HRP). In contrast, in the presence of either the PCA@ZIF-L or H_2O_2 alone, it showed almost no visible color change or characteristic absorption peak at 652 nm under the same conditions. These results successfully confirmed an intrinsic peroxidase-mimicking activity of the PCA@ZIF-L composites. For further verifying whether the POD-like property is due to PCA or ZIF-L, control groups for PCA or ZIF-L were set. As shown in Fig. S5 (Supporting information), the group (b) was colorless and the group (a) was blue, which indicated that the POD-like property of PCA@ZIF-L was resulted from PCA rather than ZIF-L.

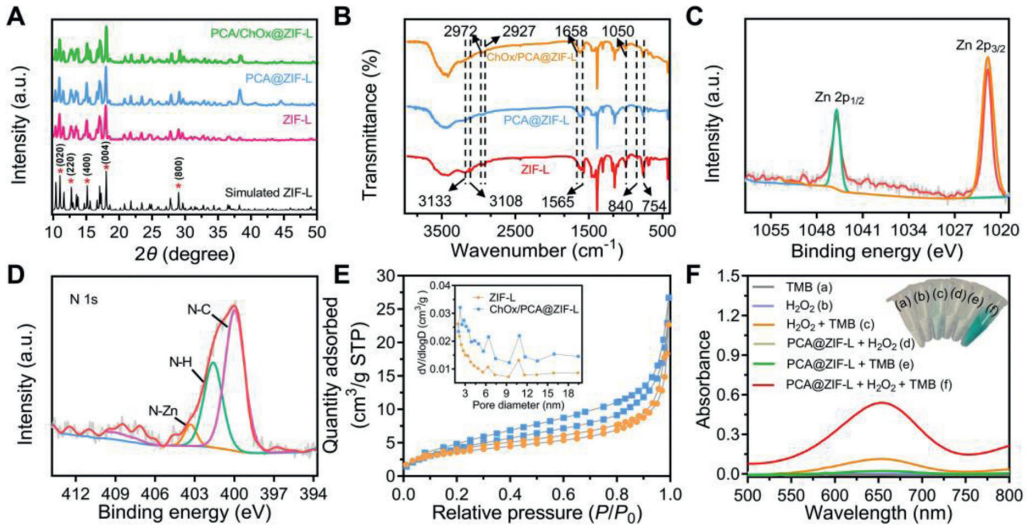

Fig. 2. (A) X-ray diffraction patterns and (B) FT-IR spectra of ZIF-L, PCA@ZIF-L, and ChOx/PCA@ZIF-L. High resolution XPS spectra of Zn 2p (C) and N 1s (D) in ChOx/PCAZIF-L. (E) The nitrogen sorption-desorption isotherms of ZIF-L and ChOx/PCA@ZIF-L. Inset: pore size distribution of ZIF-L and ChOx/PCA@ZIF-L. (F) UV−vis absorption spectra of TMB in different reaction systems. The inset of (F) shows the related digital photos.

In order to further examine the superiority of ZIF-L as an enzyme carrier, the dynamic behaviors of the immobilized enzyme in ZIF-L and ZIF-8 have been compared, because metal ions and organic linkers of them are resemblances. The PCA@ZIF-L was used because its catalytic reaction product of TMB and H_2O_2 can be easily detected. The ZIF-8 loaded PdCuAu nanoparticles (PCA@ZIF-8) was synthesized through the co-precipitation with 25 mmol/L Zn^{2+} and 25 mmol/L 2-methylimidazole. As shown in Figs. S6A and B (Supporting information), the TEM results exhibited that the prepared ZIF-8 was the standard rhombic dodecahedral morphology, and PdCuAu nanoparticles were attached to the ZIF-8 surface. It can be observed that whether using PCA@ZIF-L or PCA@ZIF-8 as a catalyst, the reaction rate increases with the addition of H_2O_2 concentration (fixed TMB concentration) or TMB (fixed H_2O_2 concentration). As illustrated in Fig. S7 (Supporting information), the typical Michaelies-Menten curves were successfully fitted using GraphPad Prism 9.0 software (California, USA), from which the Michaelis constant (K_m), the maximum reaction rate (V_{max}) and catalytic number (K_{cat}) can be calculated (Table S2 in Supporting information). The apparent K_m value of PCA@ZIF-L is 0.0864 and 0.0531 mmol/L using TMB and H_2O_2 respectively, which are lower than that of PCA@ZIF-8 (0.0968 and 0.1041 mmol/L). Compared with the previously reported nanozymes, the K_m value of as-prepared PCA@ZIF-L was 69.8 times lower than that of HRP when H_2O_2 was used as substrate (Table S3 in Supporting information). What is more, the second-order rate constant (K_{cat}/K_m) is the most important parameter to measure the catalytic efficiency of an enzyme [49]. As shown in Table S2, the K_{cat}/K_m of PCA@ZIF-L, varying the concentration of H_2O_2, was 1.79 times that of PCA@ZIF-8. The above results suggest that the PCA@ZIF-L has stronger affinity and higher catalytic efficiency to the substrate than PCA@ZIF-8. This is benefiting from superior adsorption selectivity to ChOx of ZIF-L. Furthermore, the slopes the fitted lines in Figs. S8A and B (Supporting information) were parallel, revealing a ping-pong mechanism.

As H_2O_2 is the oxidation product of cholesterol by O_2 and can oxidize TMB to produce chromogenic substance through the cascade catalytic reaction, the relationship between the UV-vis absorption spectra of TMB (0.2 mmol/L) and the concentrations of H_2O_2 is studied with the existence of 50 μg/mL ChOx/PCA@ZIF-L. It can be seen from Fig. S9A (Supporting information) that the absorbance increases with the increasing of H_2O_2 concentration, the color of the solution gradually changes from colorless to blue. The absorbance intensity at 652 nm shows a linear relationship with H_2O_2 from 0.1 mmol/L to 1.0 mmol/L, the linear equation is $A = 0.3318C_{(H_2O_2)} + 0.2808$ (Fig. S9B in Supporting information). The obtained results indicate that the ChOx/PCA@ZIF-L acts as an ideal probe for the quantification of H_2O_2, which lays the foundation for its further application for cholesterol assay.

Next, the cascade catalytic reaction efficiency of the immobilized enzymes in ZIF-L and ZIF-8 have been compared. The ZIF-8 loaded ChOx and PdCuAu nanoparticles (ChOx/PCA@ZIF-8) was synthesized through the co-precipitation with 25 mmol/L Zn^{2+} and 25 mmol/L 2-methylimidazole. The absorbance at 652 nm of each group is monitored with the time prolonging (Fig. S9C in Supporting information). It is noted that the absorbance reaches 0.46 after reaction for 30 min with the existence of ChOx/PCA@ZIF-L. However, the absorbance of the solution catalyzed by ChOx/PCA@ZIF-8 is only about 72.96% that by ChOx/PCA@ZIF-L. The above experiments suggest that the ZIF-L is more suitable for multiple enzymes' immobilization of cascade catalytic reaction. The detection conditions for cholesterol based on ChOx/PCA@ZIF-L were optimized to obtain maximum assay sensitivity. As shown in Fig. S10 (Supporting information), the relative activity continuously increases with the temperature from 25 °C to 45 °C, and begins to decrease when the temperature rises to 50 °C. A lower pH is beneficial to the cascade catalytic reactions because acidic solutions provide electrolytes that are effective in facilitating electron transfer during redox processes, however, excessive acidity (pH 3.5) may lead to the degradation of ZIF-L, making the relative activity decreasing (Fig. S11 in Supporting information). There were positive correlations between the absorbance and the concentrations of TMB (Fig. S12 in Supporting information) or ChOx/PCA@ZIF-L (Fig. S13 in Supporting information). Therefore, the assay of cholesterol was conducted under the following experimental conditions: (a) 10 μL ChOx/PCA@ZIF-L (50 μg/mL); (b) 10 μL TMB (0.2 mmol/L); (c) 870 μL NaAc-HAc buffer solution (pH 4.0); (d) incubation temperature 45 °C; (e) incubation time 30 min.

And then, the absorbance at 652 nm of the TMB with different concentration of cholesterol was measured under the optimal conditions. As shown in Fig. 3A, the absorbance was gradually enhanced with the increasing concentration of cholesterol from 0.0005 mmol/L to 1.0000 mmol/L, indicating that the relationship between the absorbance at 652 nm and cholesterol

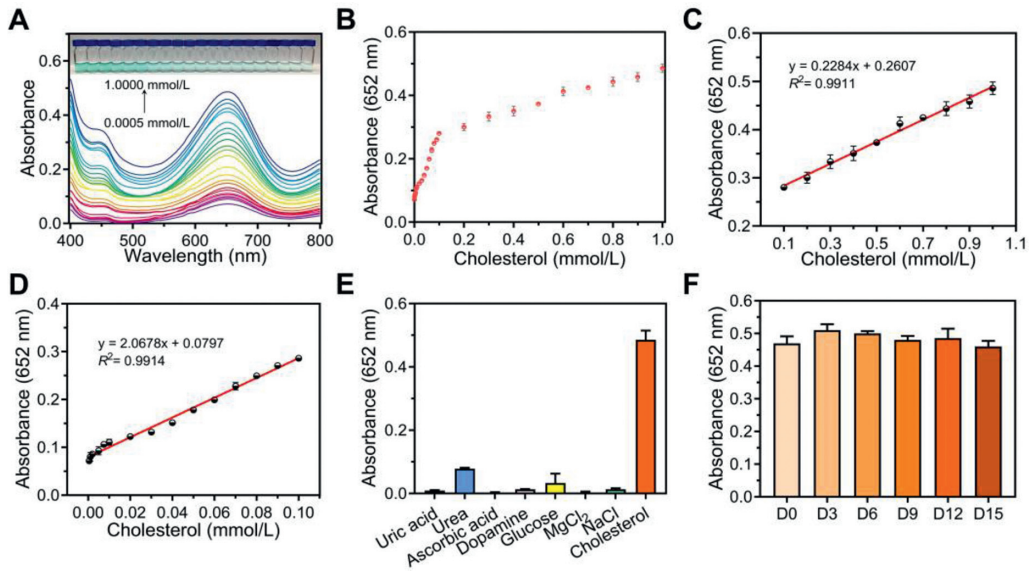

Fig. 3. (A) UV–vis spectra of colorimetric detection of cholesterol based on ChOx/PCA@ZIF-L. The inset photograph showed the colored TMB solution with varying concentrations of cholesterol. (B) Plot of the absorbance change at 652 nm *versus* the concentration of cholesterol from 0.0005 mmol/L to 1.0 mmol/L. (C, D) The calibration curve (absorbance at 652 nm) *vs.* concentration of cholesterol (0.1–1.0 mmol/L and 0.0005–0.1 mmol/L). The error bars indicated the standard deviation of three experiments. (E) Selectivity analysis for cholesterol detection. The concentrations were as follows: 1 mmol/L cholesterol, 10 mmol/L uric acid, 10 mmol/L urea, 10 mmol/L ascorbic acid, 10 mmol/L dopamine, 10 mmol/L glucose, 10 mmol/L $MgCl_2$, and 10 mmol/L NaCl. (F) The stability of the cholesterol biosensor based on the ChOx/PCA@ZIF-L every three days during a 15-day period. The error bars represented the standard deviations of three measurements.

concentration was dose-dependent (Fig. 3B). It can be seen that there was a linear relationship between the absorption at 652 nm and the concentration of cholesterol in two intervals. When the cholesterol concentration ranged between 100 μmol/L to 1000 μmol/L (Fig. 3C), the regression equation was $A = 0.2284C_{(\text{cholesterol})} + 0.2607$ ($R^2 = 0.9911$). Besides, a linear relationship ($A = 2.0678C_{(\text{cholesterol})} + 0.0797$, $R^2 = 0.9914$) between the absorbance value and the cholesterol level was calibrated in the content range from 0.5 μmol/L to 100 μmol/L (Fig. 3D), with a limit of detection (LOD) estimated to be 0.2176 μmol/L ($3\sigma/k$, where σ is the standard deviation of the blank samples, $\sigma = 0.00014$). Compared to the latter standard curve, the slope of the former linear equation had dropped, indicating that a common saturation effect was observed when more cholesterol was added. As summarized in Table S4 (Supporting information), in comparison with other cholesterol biosensors, ChOx/PCA@ZIF-L exhibited a superior or competitive analytic performance.

The selectivity of ChOx/PCA@ZIF-L-based detection approach with possible interfering substances in blood samples including uric acid, urea, ascorbic acid, dopamine, glucose, $MgCl_2$, and NaCl were investigated. Fig. 3E showed that the absorbance of these interfering substances was not evident when their concentrations were ten times as high as that of cholesterol. This indicated that the approach was probably suitable for the cholesterol determination in human blood. The stability of the detection system is another key factor in practical application. The stability of ChOx/PCA@ZIF-L sensing platform was investigated by detecting the same cholesterol concentration (1.0 mmol/L) every three days. As shown in Fig. 3F, during 15 days, there were no obvious changes in the absorbance at 652 nm, revealing that the ChOx/PCA@ZIF-L sensing platform had a good stability which was appropriate for paper-based analytical detection.

Given the determination of serum cholesterol concentration is closely related to human health, the human serum samples were applied for cholesterol assay to demonstrate the analytical reliability of the proposed strategy. As stated above, TG in serum is the sum of free cholesterol and cholesterol esters [50]. In fact, cholesterol ester can be converted to free cholesterol by cholesterol esterase effectively. Therefore, cholesterol level in human serum sample equals to free cholesterol after pretreatment by cholesterol esterase. According to the absorbance of oxTMB in serum sample, combining with dilution multiple and linear calibration plot for cholesterol, eight serum samples were added to test the cholesterol concentration using the proposed method and the standard enzymatic measurements (detected by hospital). To investigate the consistency of the two methods, Bland-Altman plot was adopted for analysis. As shown in Fig. S14 (Supporting information), the difference between the detection results of the two methods was within 95% limits of agreement (95% LoA), indicating the results of the two methods are consistent.

Although the ChOx/PCA@ZIF-L combined with UV-vis spectrophotometer have realized a sensitive and selective detection of serum cholesterol, the necessity of professional equipment making it is hard to serve as a daily monitoring tool. With the growing demands for quick, convenient, affordable on-site diagnosis, paper-based sensors rise in response to the proper time and conditions. A simple paper-based sensing system is constructed through a pre-reaction-transfer operation, which gets rid of the complex pre-processing requirements of traditional operations on filter paper. As shown in Fig. S15A (Supporting information), after removing the filter paper from the reaction system with different concentrations of cholesterol, the color could be seen to be different with the naked eye. The color images were captured using a smartphone camera, analyzed by the TakeColor APP, and the corresponding gray values were obtained by calculation. A linear relationship ($\text{Gray} = -26.4\lg(C_{(\text{cholesterol})}) + 190.0$, $R^2 = 0.9951$) between the gray value and the cholesterol level was calibrated in the content range from 0.1 mmol/L to 10 mmol/L (Fig. S15B in Supporting information).

In summary, we have successfully prepared PdCuAu NPs and ChOx self-encapsulated on ZIF-L nanosheets *in situ* by the co-precipitation method. Benefiting from its large pore size and efficient molecular transport, the ZIF-L obviously improved the efficiency of cascade catalytic reaction. The apparent K_m value of PCA@ZIF-L is calculated as 0.0864 and 0.0531 mmol/L using TMB and H_2O_2 respectively, which are lower than that of PCA@ZIF-8

(0.0968 and 0.1041 mmol/L). After reaction with 1.0 mmol/L cholesterol for 30 min, the absorbance of TMB has reached 0.46 catalyzed by ChOx/PCA@ZIF-L, while that is only 0.33 by ChOx/PCA@ZIF-8. The colorimetric biosensor based ChOx/PCA@ZIF-L exhibits high sensitivity and excellent selectivity towards serum cholesterol. More importantly, the fabricated POCT device utilizing paper sensing system and smartphone also enables frequent cholesterol monitoring to some patients with cardiovascular-related diseases.

Declaration of competing interest

The authors declare that they have no known competing financial interests or personal relationships that could have appeared to influence the work reported in this paper.

Acknowledgments

This work is supported by the National Natural Science Foundation of China (Nos. 81971765, 31771099, 31671025 and 81871504), and the Natural Science Foundation of Guangdong Province (No. 2020A1515011066).

Supplementary materials

Supplementary material associated with this article can be found, in the online version, at doi:10.1016/j.cclet.2022.05.024.

References

[1] J. Li, T. Liu, S. Liu, et al., Biosens. Bioelectron. 120 (2018) 137–143.
[2] Y. He, N. Li, W. Li, et al., Sens. Actuators B: Chem. 326 (2021) 128850.
[3] A. Pirillo, M. Casula, E. Olmastroni, et al., Nat. Rev. Cardiol. 18 (2021) 689–700.
[4] NCD Risk Factor Collaboration (NCD-RisC), Nature 582 (2020) 73–77.
[5] P. Song, Q. Man, H. Li, et al., Biomed. Environ. Sci. 32 (2019) 559–570.
[6] S. Beheshti, C. Madsen, A. Varbo, et al., J. Am. Coll. Cardiol. 75 (2020) 2553–2566.
[7] A. Varbo, M. Benn, A. Tybjerg-Hansen, et al., J. Am. Coll. Cardiol. 61 (2013) 427–436.
[8] R. Villanueva, M. Plaza, M. Garcia, et al., Microchem. J. 156 (2020) 104812.
[9] L. Yang, H. Zhao, Y. Li, et al., Analyst 141 (2016) 270–278.
[10] U. Saxena, M. Chakraborty, P. Goswami, Biosens. Bioelectron. 26 (2011) 3037–3043.
[11] T. Han, S. Zhu, S. Wang, et al., Microchim. Acta 186 (2019) 269.
[12] H. Xu, Y. Zhao, Y. Tan, ACS Appl. Mater. Interfaces 11 (2019) 27233–27242.
[13] T. Lin, L. Zhong, H. Chen, et al., Microchim. Acta 184 (2017) 1233–1237.
[14] C. Hong, X. Zhang, C. Wu, et al., ACS Appl. Mater. Interfaces 12 (2020) 54426–54432.
[15] L. Zhao, Z. Wu, G. Liu, et al., J. Mater. Chem. B 7 (2019) 7042–7051.
[16] X. Zhang, Q. Yang, Y. Lang, et al., Anal. Chem. 92 (2020) 12400–12406.
[17] S. Huang, X. Kou, J. Shen, et al., Angew. Chem. Int. Ed. 59 (2020) 8786–8798.
[18] V. Pandey, J. Rani, N. Jaiswal, et al., Int. J. Biol. Macromol. 104 (2017) 1713–1720.
[19] Y. Liu, R. Lv, S. Sun, et al., Chin. Chem. Lett. 33 (2022) 807–811.
[20] Y. Zhang, Q. Yue, M. Zagho, et al., ACS Appl. Mater. Interfaces 11 (2019) 10356–10363.
[21] Y. He, X. Niu, L. Shi, et al., Microchim. Acta 184 (2017) 2181–2189.
[22] W. Shi, H. Fan, S. Ai, et al., Sens. Actuators B: Chem. 221 (2015) 1515–1522.
[23] J. Qiao, L. Liu, J. Shen, L. Qi, Chin. Chem. Lett. 32 (2021) 3195–3198.
[24] X. Gao, Y. Ding, Y. Sheng, et al., ChemCatChem 11 (2019) 2828–2836.
[25] Q. Wang, D. Astruc, Chem. Rev. 120 (2020) 1438–1511.
[26] Z. Zhao, Y. Huang, W. Liu, et al., ACS Sustain. Chem. Eng. 8 (2020) 4481–4488.
[27] Y. Zhang, B. Yan, Nanoscale 11 (2019) 22946–22953.
[28] P. Gao, M. Shi, R. Wei, et al., Chem. Commun. 56 (2020) 924–927.
[29] X. Wang, P. Lan, S. Ma, ACS Cent. Sci. 6 (2020) 1497–1506.
[30] H. Xiao, H. Zhou, S. Feng, et al., J. Membr. Sci. 619 (2021) 118782.
[31] W. Liu, Y. Ban, J. Liu, et al., Sep. Purif. Technol. 276 (2021) 119085.
[32] J. Cui, Y. Feng, T. Lin, et al., ACS Appl. Mater. Interfaces 9 (2017) 10587–10594.
[33] J. Liu, Z. Guo, K. Liang, Adv. Funct. Mater. 29 (2019) 1905321.
[34] X. Wang, L. Hu, J. Electrochem. Soc. 167 (2020) 037535.
[35] M. Dhawane, A. Deshpande, R. Jain, et al., Sens. Actuators B: Chem. 281 (2018) 72–79.
[36] J. Liu, Z. Geng, Z. Fan, et al., Biosens. Bioelectron. 132 (2019) 17–37.
[37] J. Chen, H. Gao, Z. Li, et al., Chin. Chem. Lett. 31 (2020) 1398–1401.
[38] Y. Zhou, Z. Chen, S. Zeng, et al., ACS Appl. Mater. Interfaces 13 (2021) 53659–53670.
[39] Y. Chen, Y. Yang, A. Orr, et al., Angew. Chem. Int. Ed. 60 (2021) 17164–17170.
[40] X. Wang, S. Choi, L. Roling, et al., Nat. Commun. 6 (2015) 7594.
[41] D. Chen, P. Sun, H. Liu, et al., J. Mater. Chem. A 5 (2017) 4421–4429.
[42] S. Shrestha, B. Wang, P. Dutta, Adv. Colloid Interface Sci. 279 (2020) 102162.
[43] P. Yang, Q. Ren, Y. Chen, et al., New J. Chem. 45 (2021) 19565–19571.
[44] P. Yang, J. Tao, F. Chen, et al., Small 17 (2021) 2005865.
[45] Z. Liu, Q. Wu, F. Vriesekoop, et al., ACS Biomater. Sci. Eng. 5 (2019) 6581–6589.
[46] P. Raju, P. Arivalagan, S. Natarajan, J. Photochem. Photobiol. B 203 (2020) 111774.
[47] X. Liu, W. Qi, Y. Wang, et al., Nanoscale 9 (2017) 17561–17570.
[48] R. Chen, J. Yao, Q. Gu, et al., Chem. Commun. 49 (2013) 9500–9502.
[49] S. Liu, S. Qiao, T. Yan, et al., Chem. Eng. J. 429 (2022) 132592.
[50] X. Sun, Y. Zhang, D. Zheng, et al., Biosens. Bioelectron. 92 (2017) 81–86.